JGR Solid Earth

RESEARCH ARTICLE
10.1029/2019JB017479

# Origin of Long-Wavelength Magnetic Anomalies at Subduction Zones

**Simon E. Williams**[1,2] **and David Gubbins**[2,3,4]

[1]State Key Laboratory of Continental Dynamics, Department of Geology, Northwest University, Xi'an, China, [2]School of Geosciences, University of Sydney, Sydney, New South Wales, Australia, [3]School of Earth and Environment, University of Leeds, Leeds, UK, [4]Space Science Institute, Macau University of Science and Technology, Macau

**Abstract** Most subduction zones have associated long-wavelength anomalies in the lithospheric magnetic field observed at satellite altitude. We model the 13 subduction zones defined by seismicity and seismic tomography using vertically integrated magnetizations that are increasing, level, or decreasing away from the trench. These mimic end members of a magnetized mantle wedge, a uniform layer, and a magnetized dipping lithospheric slab. They are added to a global model of vertically integrated magnetization based on continental and oceanic geology. We find the dipping slab places the anomaly too close to the trench, while the other two fit the data equally well and use the level model in the main part of the study. Anomalies at the Sunda, Aleutians, Cascadia, Central American, and Kamchatka-Japan zones are well modeled by uniform magnetization of differing susceptibilities and spatial extents. We show the South American anomaly is weak because the magnetization lies mainly in the null space that produces no external potential magnetic field. There is no anomaly associated with the Ryukyu system, possibly because the present subduction started too recently for magnetization to have formed. The magnetic anomaly stretching down the Baja California peninsula is not present in the prediction because there is no seismicity on which to base a slab geometry, but recent tomography suggests a fossil slab there and we propose historic subduction as the origin of the Baja magnetic anomaly. Finally, we discuss the mineralogical origins of the magnetization and favor serpentinization of the region above the subducted plate.

**Key Points:**
- Many subduction zones are associated with long-wavelength magnetic anomalies
- The anomalies are unlikely to be explained by magnetization solely in the subducting slab
- Modeling supports the hypothesis of magnetized serpentinite in the mantle wedge

**Supporting Information:**
- Supporting Information S1

**Correspondence to:**
S. Williams,
simon.williams@nwu.edu.cn

**Citation:**
Williams, S. E., & Gubbins, D. (2019). Origin of long-wavelength magnetic anomalies at subduction zones. *Journal of Geophysical Research: Solid Earth*, *124*, 9457–9473. https://doi.org/10.1029/2019JB017479

Received 31 JAN 2019
Accepted 10 AUG 2019
Accepted article online 15 AUG 2019
Published online 3 SEP 2019



## 1. Introduction

The component of the geomagnetic field observed at satellite altitudes above spherical harmonic degree 15 or so shows complex anomalies, thought to arise predominantly from magnetized minerals in the Earth's crust and lithosphere at shallow depths where the rock temperature is below the Curie temperature for important magnetic minerals. However, many of these anomalies remain unexplained and determining the magnetization responsible is difficult because of a fundamental ambiguity: Different structures produce identical magnetic fields, while others produce no magnetic field at all (Maus & Haak, 2003; Runcorn, 1975). The inverse problem for magnetization from magnetic field data is therefore highly nonunique: The null space is large, particularly if the magnetization is remanent. Inversion in the presence of such large null spaces is dangerous because even the slightest effort to regularize the solution results in elimination of the complete null space, which will inevitably contain important geological structures. Therefore, most studies that employ magnetic surveys use them to complement geological studies based on other data rather than using magnetism in isolation.

Hemant and Maus (2005) adopted a global, forward modeling approach to construct a map of continental magnetization from the United Nations Educational, Scientific and Cultural Organization world geological map (Commission for the Geological Map of the World, 2000) and tables of susceptibilities (Clark & Emerson, 1991; Hunt et al., 1995). Masterton et al. (2013) added a model of oceanic magnetization by computing an induced component for the crust and plausible remanence. Remanence was calculated by creating it at the ridges during plate formation, rotating them into their present positions, and allowing for thermal and chemical changes in the remanence with time.

These models reproduce many features in the magnetic field as observed by satellites quite well, for example, anomalies within continents where the geology is well known and the signal due to the boundaries of the Cretaceous Normal Superchron (CNS) within oceanic lithosphere. However, there are significant misfits,

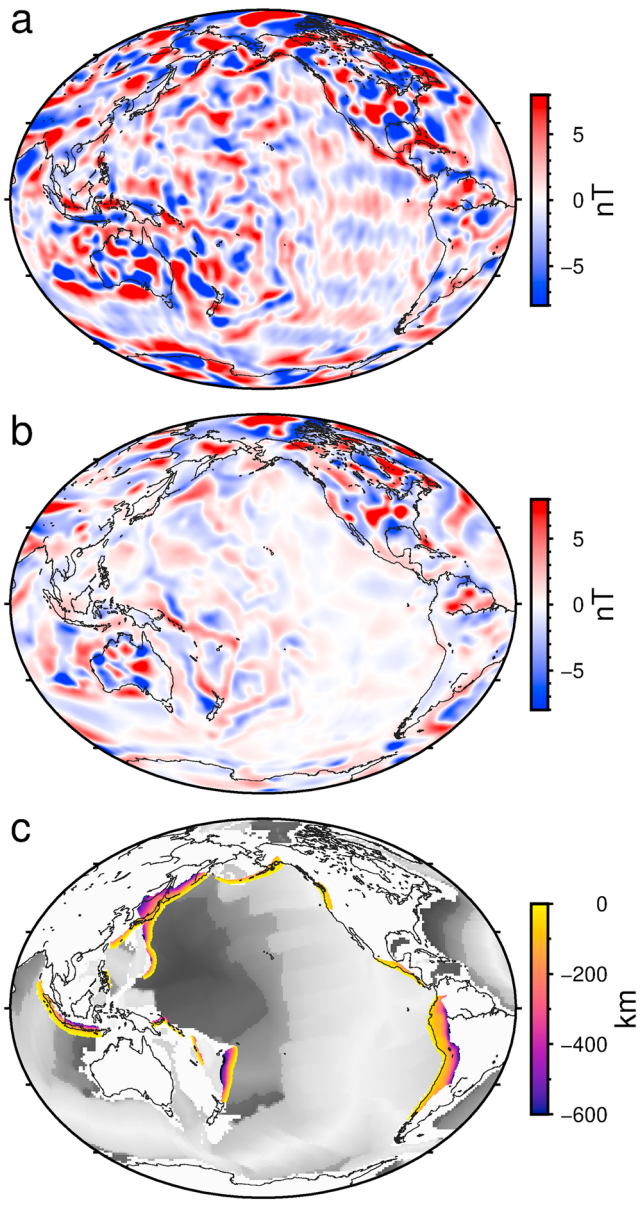


**Figure 1.** (a) Vertical component of magnetic field from model MF7 (see http://www.geomag.us/models/MF7.html) at 300-km altitude, (b) prediction from the base model of Masterton et al. (2013), and (c) subduction zones of model Slab1.0 of Hayes et al. (2012), defined by seismicity. The shading in the oceans represents the age of the seafloor from light gray (young) to dark gray (old); discontinuities in the gray scale highlight the edges of the Cretaceous Normal Superchron.

some obvious ones arising from structures absent from the model: The interior of Antarctica has virtually no geological information in the world map, large igneous provinces, and oceanic plateaux are treated as ordinary continent, and there are no subduction zones. Anomalies that appear to be associated with each of these features show up in satellite magnetic field models (Figure 1). Here we add subduction zones to the global model.

It has long been recognized that subduction zones contribute to satellite magnetic field observations (Frey, 1982). High-quality MAGSAT data were used to create magnetization models of the Aleutian Arc (Clark et al., 1985) and Middle America Trench (Vasicek et al., 1988). They attributed the anomalies to magnetization of the cold, subducted plate contrasting with the hotter and therefore nonmagnetic, surrounding mantle. Arkani-Hamed and Strangway (1987) compared several subduction zones and found that older subducting lithosphere produced stronger magnetic anomalies than younger subducting lithosphere, as did those at high geomagnetic latitude compared to those at low latitudes. In particular, the Aleutian Arc has a strong magnetic anomaly, while that above the Peru-Chile Arc is very weak. More recently, Blakely et al. (2005) proposed an alternative scenario for the Cascadia subduction zone in which a magnetized, serpentinized wedge above the subducted plate yielded a good match with the long-wavelength component of aeromagnetic data. Anomalies are also expected at ocean-continent boundaries and where old and young oceanic plates meet; these show up in satellite magnetic field models in some places (Counil et al., 1991; Masterton et al., 2013), complicating the interpretation of signatures due to the subducting slab and wedge.

Our approach here follows that of Gubbins et al. (2011) and Masterton et al. (2013), who use vector spherical harmonics (VSH) to separate the "visible" part of the magnetization from the null space, that part of the magnetization which generates no external potential magnetic field. Details of the method are given in Gubbins et al. (2011). We use it here to determine whether a particular subduction zone magnetization fails to generate an anomaly because it falls within the null space. The method reveals whether a particular subduction zone will produce a large or small anomaly based on its geomagnetic latitude and orientation, possibly explaining some of the differences noted by Arkani-Hamed and Strangway (1987). For all models in this study, we use the global model of Masterton et al. (2013) as the "base model." The subduction zone magnetization is added to this base model and its computed magnetic field at satellite altitude compared with a lithospheric magnetic field model derived from satellite observations.

Magnetization of the downgoing slab (e.g., Clark et al., 1985) and overlying mantle wedge (Blakely et al., 2005) produce quite different vertically integrated magnetizations (VIMs) since that of the slab decreases away from the trench while that of the wedge increases. We employ two very simple models of VIM whose magnetizations decrease and increase away from the trench, respectively, and a third intermediate model with uniform magnetization. The planform of the VIM is determined by seismicity and seismic tomography of the subduction zones. We compare the magnetic fields generated against satellite model MF7 (an updated version of the MF6 model described by Maus et al., 2008) in order to discriminate between the alternative scenarios and end with a discussion of possible mineralogical origins of subduction zone magnetism.

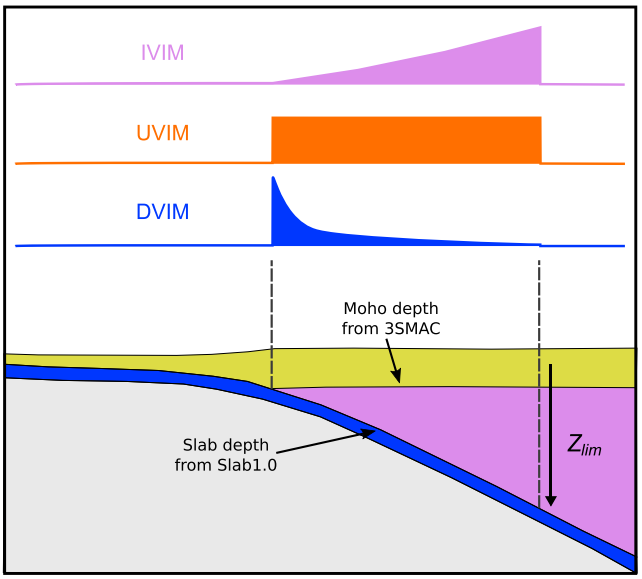


**Figure 2.** Schematic cross section illustrating the three different VIM models considered in this study. The IVIM model assumes that magnetization increases away from the trench as the thickness of the mantle wedge increases, until the limiting depth $Z_{\mathrm{lim}}$ is reached. The UVIM model adds uniform magnetization to the region between the trench and location of the slab contour defined by $Z_{\mathrm{lim}}$. The magnetization for DVIM models decreases rapidly away from the trench, representing the cases where the slab is the main source of magnetization.

## 2. Methods

Three-dimensional locations and geometries of subduction zones are defined by model Slab1.0 of Hayes et al. (2012; see Figure 1, their Table 1, and Figure 1c). The Slab1.0 data set comprises 13 subducting slabs. The Scotia arc proved too small to provide a magnetic anomaly based on our magnetization models and since it does not appear either in the MF7 model it was removed from this study. The slab geometries are based mainly on seismicity plus some tomographic models, smoothed and interpolated onto a 0.5° grid. The seismogenic zones vary in thickness from 50 to 150 km. In addition to slab geometry, seismicity is also an indicator of cold temperature in the subducted slab and therefore the thickness of any possible magnetized zone.

The extent of magnetization in subduction zones is controlled by temperature and specifically the location of the Curie isotherm. Therefore, to determine the range of magnetization depths to investigate in our models, we looked to thermal models (Kincaid & Sacks, 1997; Syracuse et al., 2010) accounting for factors such as convergence rates, downgoing plate age, insulating effects of slab sediments, and variations in upper plate properties provide a useful guide to the expected temperature distribution. A Curie temperature for magnetite of 580 °C (Clark, 1997) gives a limit of the extent of any magnetization at depth, whether in the slab or wedge above it. The influence of pressure may raise the Curie temperature by ~20 °C at lower crustal/upper mantle depths (ter Maat et al., 2019). The thermal models of Syracuse et al. (2010) suggest that within subduction zones, the deepest extent of the Curie isotherm at or below the slab Moho varies significantly between different trenches and may lie anywhere between 50 and 250 km in depth. Therefore, our models consider a range of scenarios with magnetization distributions spanning this range of depths.

We wish to discriminate between the two contrasting hypotheses for the source of magnetism: the downgoing slab (Clark et al., 1985) or overlying plate (Blakely et al., 2005). To this end, we construct three separate VIMs for each subduction zone (illustrated schematically in Figure 2), one that decreases with distance from the trench (DVIM, a “slab” model), one that increases (IVIM, a “wedge” model), and an intermediate case with constant magnetization (UVIM, a “uniform” model). The physical basis for the UVIM model is less clear than for the other two but can be broadly taken to represent scenarios where magnetization is distributed both within parts of the wedge and the downgoing lithosphere adjacent to it, without any systematic increase or decrease in VIM toward or away from trench. The increase in magnetization of IVIM is computed from the thickness of the wedge, where the base of the wedge is defined by the depth to the top of the slab from Slab1.0 and the top of the wedge is defined by the Moho depth of the 3SMAC model

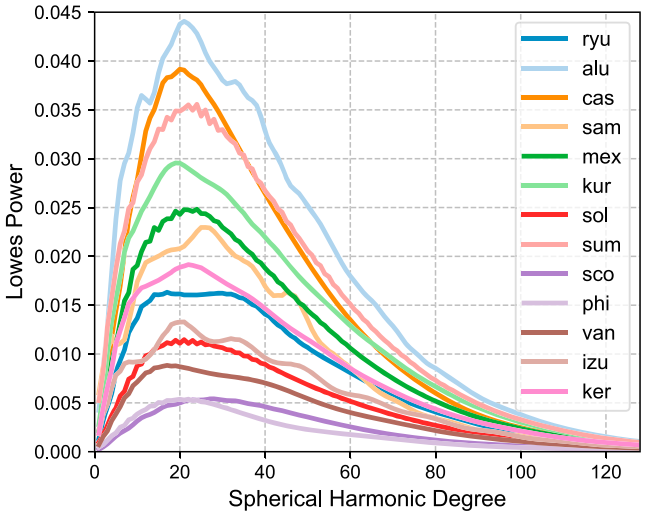


**Figure 3.** Lowes-Mauersberger spectra for individual subduction zones at satellite altitude. These all peak near $l = 20$, the value we use in assessing the reducing effect of magnetization at depth.

(Nataf & Ricard, 1996). The decrease of DVIM is determined by the factor $r'^l$ in the integrals for the moments of magnetization $\bar{\boldsymbol{M}}_l$ (see equations (8–10) of Gubbins et al., 2011), where $r$ is the radius of the magnetic element and $l$ the spherical harmonic degree. Clearly, the full range of $l$ needs to be included for a precise calculation, but that would complicate the model excessively. A simple approximate DVIM is obtained by using a single moment corresponding to the dominant spherical harmonic degree for the subduction zones, $l \approx 20$ (Figure 3). IVIM has a roughly linear increase, following the thickness of the wedge, whereas DVIM decreases very sharply: the depth factor is always less than 1 and raising it to a high power decreases it dramatically.

Each model is given two variable parameters, the volume susceptibility $k$ and a spatial parameter $Z_{\text{lim}}$. The parameter $Z_{\text{lim}}$ defines a depth contour on the slab, so that for any given model magnetization is assumed to only lie either within or above parts of the slab that are shallower than this contour; that is, VIM lies between the trench and this contour (see Figure 2). We assume that the contribution of remanent magnetic striping in oceanic lithosphere averages out to 0 at satellite altitude (Clark et al., 1985) and neglect spatial variations in magnetization within the slab and wedge, and $k$ is multiplied by the local field (Finlay et al., 2010) to produce a magnetization. For IVIM the magnetization is multiplied by the wedge thickness at each grid node; for UVIM it is multiplied by a nominal 20 km, representative of the mean thickness used for IVIM, and DVIM is normalized so the vertically integrated susceptibility at the trench end is 20 km times $k$.

We added the new VIMs into the base model and computed the new magnetic anomalies for a variety of susceptibilities $k$ and lengths $Z_{\text{lim}}$. The full vector root-mean-square (RMS) misfit to the MF7 satellite field at 300-km altitude was calculated using all grid nodes within a distance of 100 km around each subduction zone and normalized by dividing by the equivalent misfit of the base model. We located the minimum RMS to derive optimum values of susceptibility and length (Table 1 for all models and Figure 4 for the UVIM case). Each optimal magnetic structure is decomposed into the three VSH components (Gubbins et al., 2011) to determine whether the geometry and orientation of the magnetization is capable of generating a strong magnetic anomaly.

## 3. Results

### 3.1. Comparison of IVIM, UVIM, and DVIM Models

Goodness of fit to the satellite field MF7 is assessed quantitatively from the RMS misfit and qualitatively by visual comparison of the maps. For the RMS calculation all three components of the magnetic field are used, while for visual comparisons we focus on the vertical component.

Table 1 gives the RMS misfits for 12 of the subduction zones. The uniform model gives the best fits overall but is not significantly better than the wedge model. The slab model is substantially worse for all zones and $Z_{\text{lim}}$ is unrealistically large, tending toward the maximum value considered (400 km) for most zones.

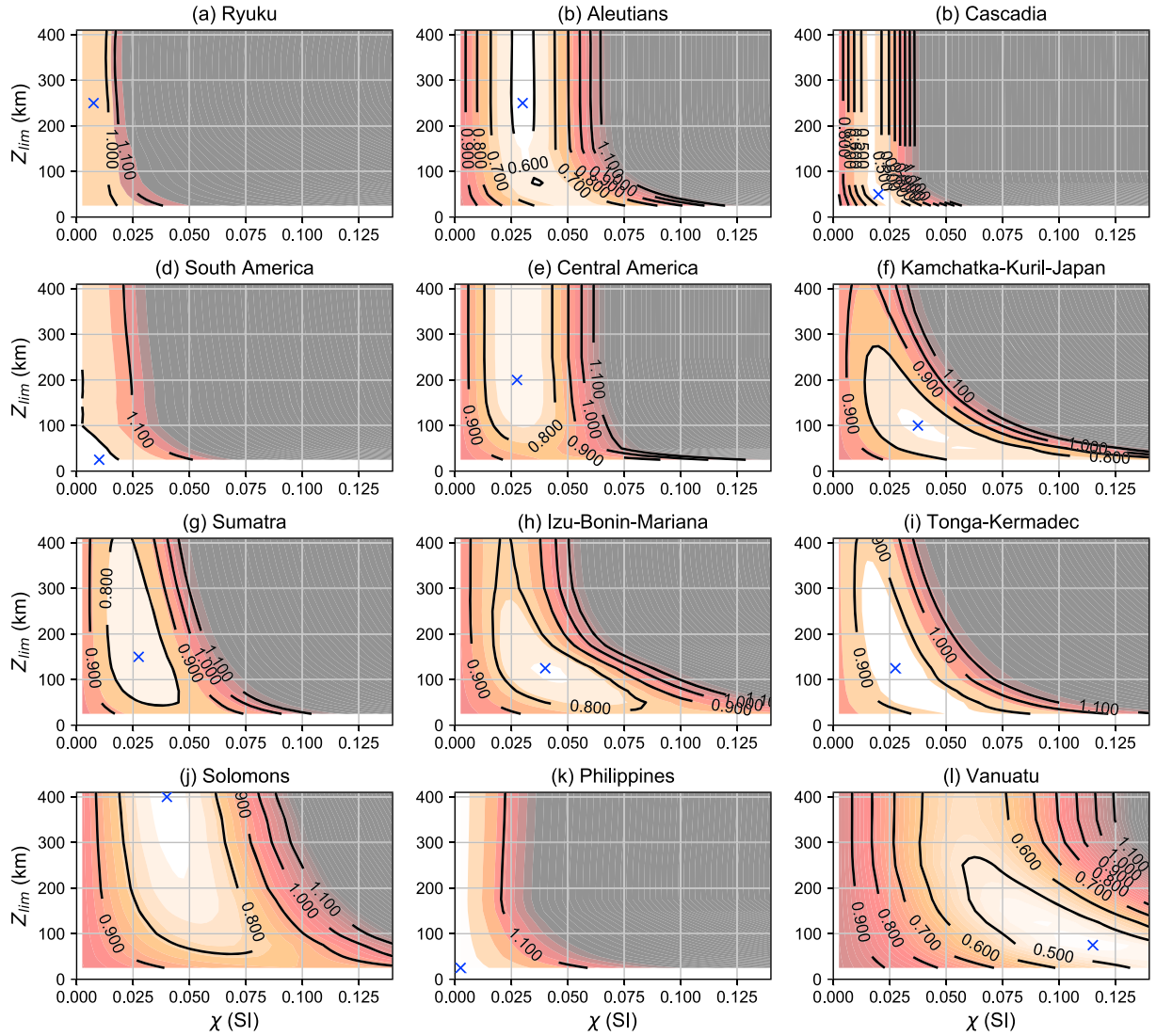


**Figure 4.** RMS contours for the UVIM models for (a–l) 12 subduction zones that were large enough to produce a meaningful minimum defining an optimal model. The root-mean-square values are computed using the full vector misfit to the MF7 satellite field at 300-km altitude, calculated for all grid nodes within a distance of 100 km of the subduction zone (as defined in Slab1.0). Values are normalized by dividing by the equivalent misfit computed in the same way for the base model.

A visual comparison of the three types of VIM model is illustrated for the Aleutian and Sumatra arcs in Figure 5. The Aleutian DVIM anomaly has a peak displaced toward the south, which explains why the RMS is large. Sumatra shows a similar effect, with UVIM and IVIM replicating the data better than DVIM. There is little difference between UVIM and IVIM, either visually or in the RMS values (Table 1), although UVIM has larger $Z_{\text{lim}}$s and there is a hint in the figures that the anomaly is displaced slightly downdip from the trench compared to IVIM (Figure 5). From here onward we focus on results for the simpler UVIM model.

Results for the RMS fit of UVIM as a function of susceptibility $k$ and length $Z_{\text{lim}}$ are shown in Figure 4. The optimum susceptibility $k$ and length $Z_{\text{lim}}$ are shown as blue crosses. The four subduction zones with the largest RMS must be considered failures: Ryukyu, South America, Tonga-Kermadec, and the Philippines. These are discussed in detail in the next section. The elongation of the contours in Figure 4 at larger values of $Z_{\text{lim}}$ reflects how increasing the length beyond a certain point will produce increasingly small reductions to the RMS. This is because the maximum depth extent of each subduction zone varies along strike, and as the value of $Z_{\text{lim}}$ is increased, it begins to exceed the maximum depth extent in parts of the slab, then eventually everywhere on the slab so that further increasing $Z_{\text{lim}}$ has no effect on the model. The best fitting values for $Z_{\text{lim}}$ are typically 200 km or less. Exceptions are Ryukyu and the Philippines, where the improvement to the

**Table 1**
*Statistical Results for Subduction Zones*

| Subduction zone | UVIM | | | IVIM | | | DVIM | | |
|---|---|---|---|---|---|---|---|---|---|
| | RMS | $k$ (SI) | $Z_{lim}$ (km) | RMS | $k$ (SI) | $Z_{lim}$ (km) | RMS | $k$ (SI) | $Z_{lim}$ (km) |
| Ryuku | 0.923 | 0.0075 | 250 | 0.916 | 0.0025 | 150 | 0.995 | 0.020 | 50 |
| Aleutians | 0.584 | 0.0300 | 250 | 0.622 | 0.045 | 50 | 0.798 | 0.060 | 400 |
| Cascadia | 0.401 | 0.0200 | 50 | 0.435 | 0.06 | 25 | 0.500 | 0.045 | 400 |
| South America | 0.994 | 0.0100 | 25 | 0.994 | 0.015 | 25 | 0.990 | 0.020 | 400 |
| Central America | 0.702 | 0.0275 | 200 | 0.680 | 0.0150 | 125 | 0.848 | 0.0725 | 400 |
| Kamchatka-Kuril-Japan | 0.708 | 0.0375 | 100 | 0.717 | 0.0525 | 50 | 0.812 | 0.080 | 400 |
| Sumatra | 0.734 | 0.0275 | 150 | 0.736 | 0.0175 | 100 | 0.850 | 0.055 | 400 |
| Izu-Bonin-Mariana | 0.714 | 0.0400 | 125 | 0.708 | 0.035 | 75 | 0.879 | 0.070 | 400 |
| Tonga-Kermadec | 0.854 | 0.0350 | 75 | 0.851 | 0.025 | 75 | 0.893 | 0.0625 | 400 |
| Solomons | 0.706 | 0.0400 | 400 | 0.685 | 0.0225 | 150 | 0.822 | 0.1275 | 400 |
| Philippines | 1.000 | 0.0000 | 0 | 1.000 | 0.0000 | 0 | 1.000 | 0.0000 | 0 |
| Vanuatu | 0.422 | 0.115 | 75 | 0.417 | 0.095 | 75 | 0.547 | 0.145 | 400 |

*Note.* Root-mean-square (RMS) is the smallest misfit of the vector magnetic field between subduction model and MF7 normalized by the RMS for the base model, both taken over a region containing the subduction zone. $k$ and $Z_{lim}$ are the optimum parameters producing the smallest RMS.

fit is negligible, and the Aleutians, where the RMS is similar for models with values of $Z_{lim}$ between 75 km and the optimal value of 250 km. Optimal values for $k$ fall in the range 0.025 to 0.045 SI, except for the poorly fitting cases of Ryukyu and South America, and for Vanuatu as discussed below.

### 3.2. Sumatra

Results for the Sunda arc are shown in Figure 6. The MF7 map exhibits an anomaly along its entire length, negative in sign and with higher amplitude in the eastern half. Such a negative anomaly is absent in the base model, while the addition of a magnetized layer coincident with the extent of the subduction zone defined by Slab1.0 (b) clearly improves the fit to the observations (a). This is reflected in over 20% reduction in RMS residual in Figure 4.

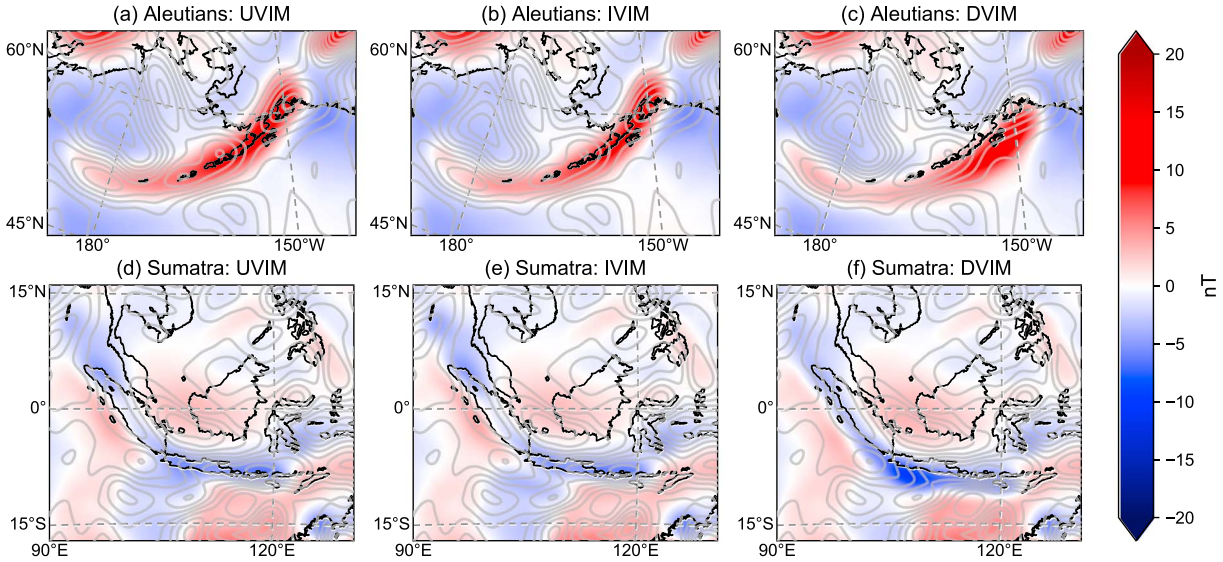


**Figure 5.** Maps of the vertical component magnetic anomaly at 300-km altitude for three different magnetization models across the Aleutian (a–c) and Sumatra (d–f) subduction zones. The gray contours represent the vertical component for the MF7 model with a contour interval of 2.5 nT. Note the displacement of the DVIM peak compared to both the other two cases and the MF7 contours.

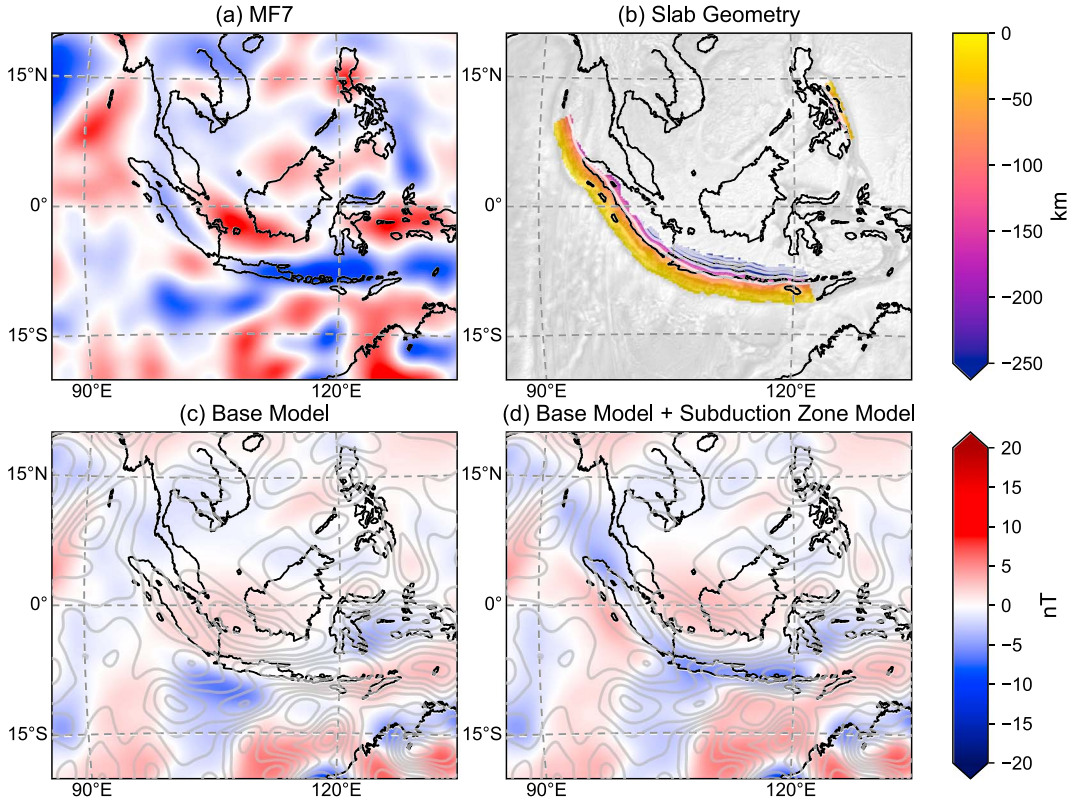


**Figure 6.** Magnetic anomalies and their predictions for the Sunda arc. (a) Subduction zone defined by seismicity and tomography from Slab1.0 (Hayes et al., 2012); (b) vertical component magnetic anomaly from observations, model MF7; (c) predictions from base model, the magnetization model of Masterton et al. (2013); and (d) predictions from subduction zone model added to the base model. Contours on (b) and (c) are of magnetic anomaly MF7 for comparison with (a).

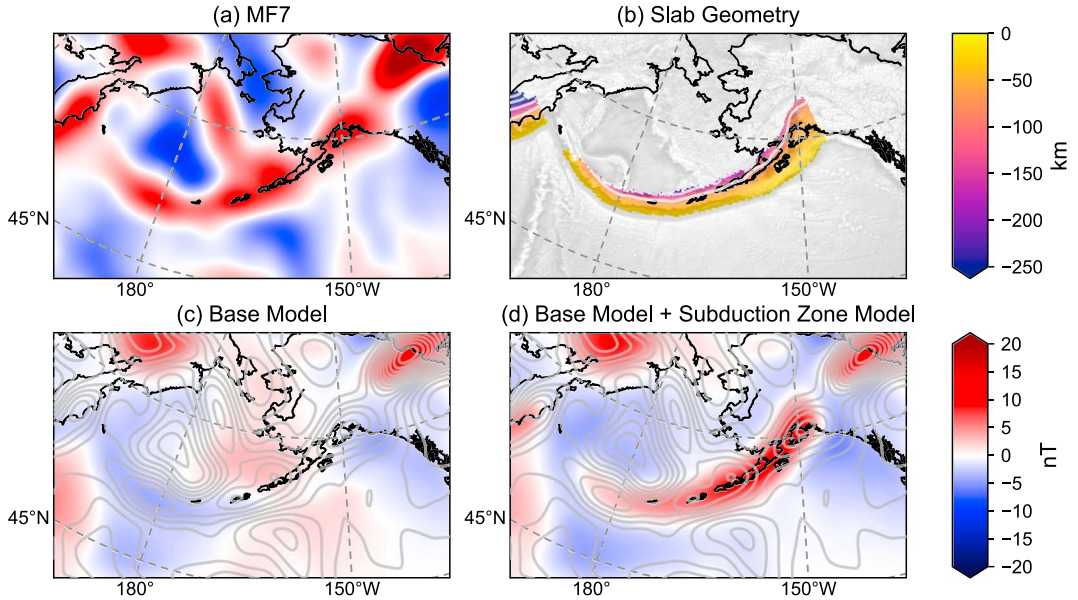


**Figure 7.** As Figure 6 but for the Aleutian subduction zone.

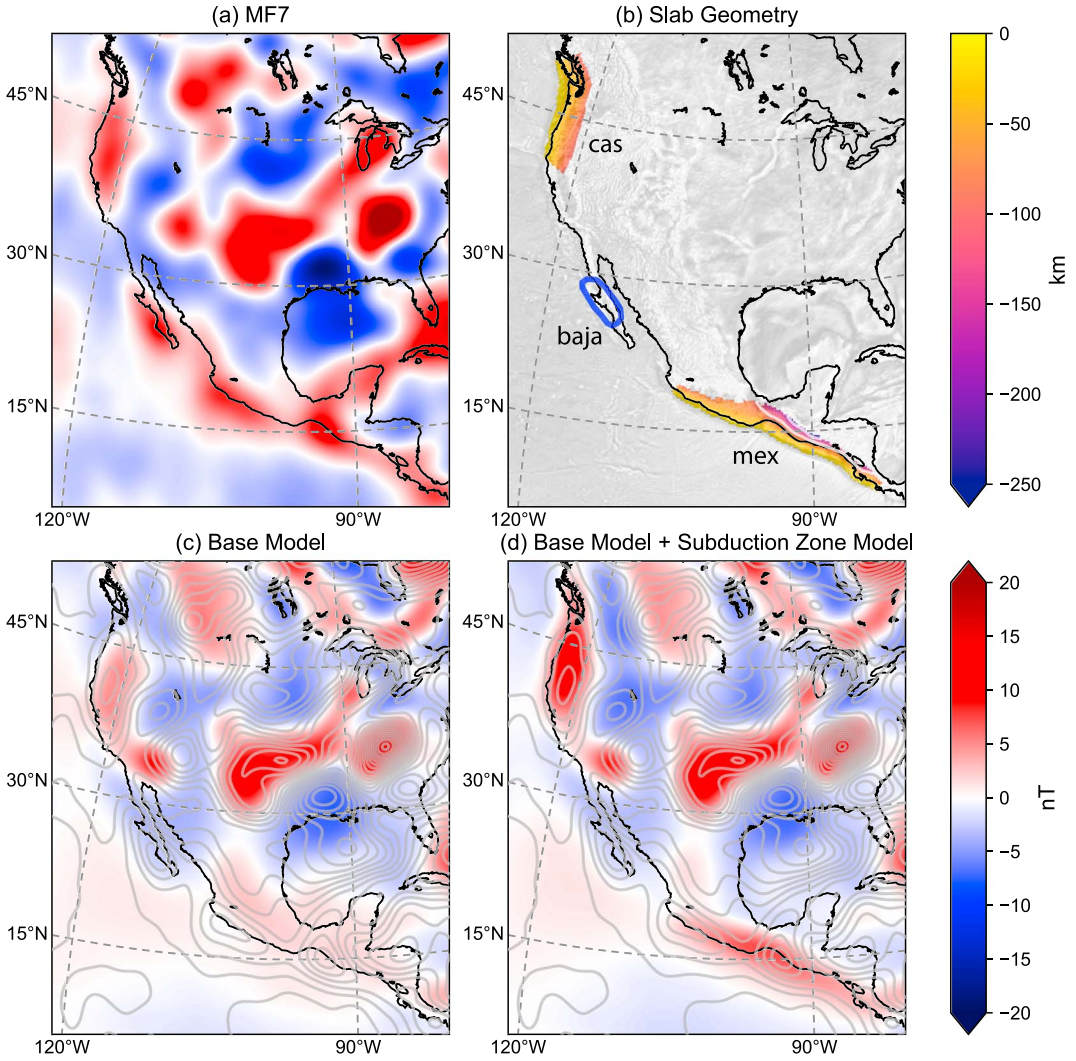


**Figure 8.** As Figure 6 but for western North America, showing both the Cascadia (cas) and Central America (mex) subduction zones. The blue outline in (b) defines the extent of the positive velocity anomaly at 100-km depth beneath Baja California interpreted as a fossil slab by Wang et al. (2013).

The base model does show a trend following the trench, but on close inspection it is seen to be the wrong sign—in this case positive instead of negative. This feature is common among several of the subduction zones we have studied. These regions typically correspond to places where the base model of Hemant and Maus (2005) incorporates regions of "arc crust," which has a low VIM. A negative anomaly observed in the MF7 map within an area of ocean south of the trench corresponds to crust formed during the CNS and is reproduced in both the base model and models with magnetization added at the slab location.

### 3.3. Aleutians

Results for the Aleutians (Figure 7) are similar to those for Sunda, with good agreement between the subduction model and satellite field in both location and strength. Once again, the base model has a weak signal along the trend of the subduction boundary with the opposite sign to that observed in the MF7 anomaly map. The spur visible in the observations north of the boundary is thought to be a result of earlier subduction, dating from before 60 Ma (Clark et al., 1985).

### 3.4. Western North and Central America

Figure 8 shows a combination for the Cascadia and Central American subduction zones. The base model shows quite good agreement over Cascadia, where a positive anomaly corresponds to locally higher values in the continental vertically integrated susceptibility of Hemant and Maus (2005). The modeled signature

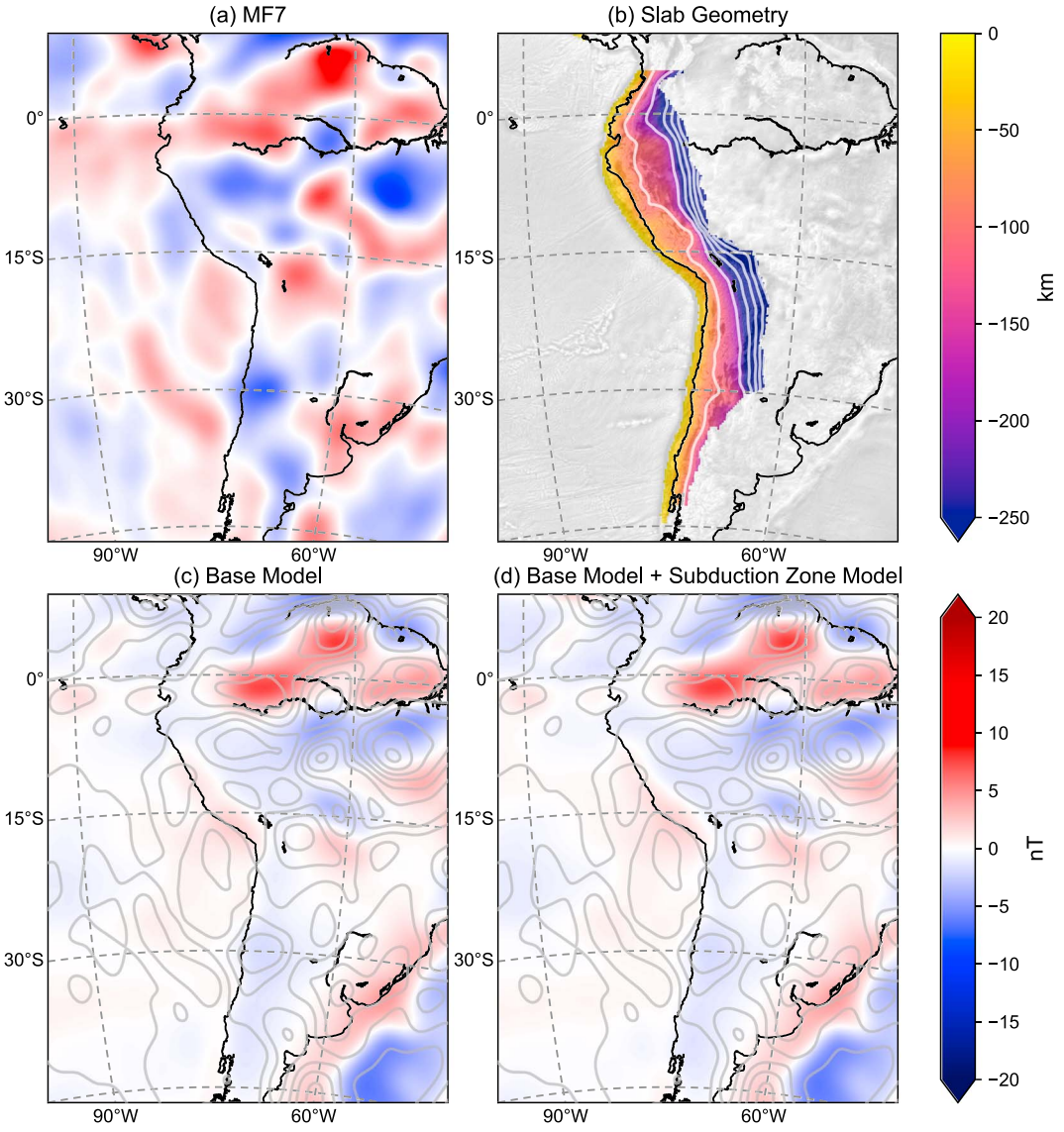


**Figure 9.** As Figure 6 but for the South American subduction zone.

of the Cascadia slab matches the observed anomaly well but produces relatively little improvement in the RMS over the base model. This is because the base model already contains a significant anomaly there; the subduction magnetism boosts its anomaly slightly.

By contrast, the base model lacks the anomaly associated with the Central American zone (Vasicek et al., 1988), and the magnetization model that incorporates this subduction zone produces a good match both visually and in terms of a reduced RMS. Slab1.0 contains no subduction zones on the western margin of the Americas between Cascadia and Central America, but subduction is thought to have been continuous along this stretch of continental margin until as recently as the Miocene (Schellart et al., 2010); recent tomography has imaged remnants of this past subduction at depths of around 100 km (Wang et al., 2013). A distinct positive magnetic anomaly in MF7 is observed in the region of Baja California that is not explained by the base model and corresponds well with the inactive subduction and fossil slab. We therefore propose that magnetization associated with this recently active subduction zone is responsible for the satellite magnetic anomaly, discussed further below.

### 3.5. South America

The lack of a strong anomaly along the West Coast of South America (Figure 9) has been noted by Arkani-Hamed and Strangway (1987), who attributed it to low geomagnetic latitude and young subduction.

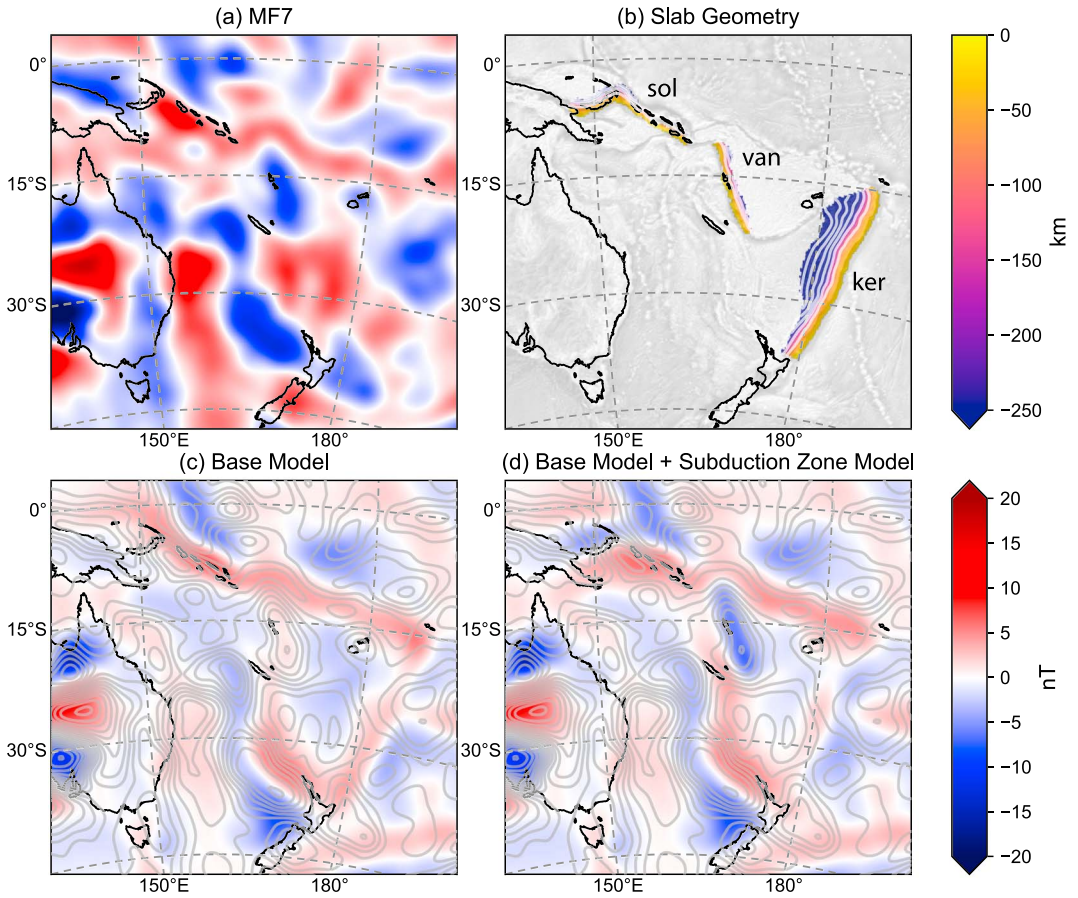


**Figure 10.** As Figure 6 but for the Tonga-Kermadec (ker), Vanuatu (van), and Solomons (sol) subduction zones.

The RMS results (Figure 4) illustrate that any significant addition of magnetization in the region of the slab causes a greater mismatch between the model and MF7 compared to the base model. We show in the next section that this results from the geometry of the magnetization: Our subduction magnetization lies in the null space and produces very little signal.

### 3.6. Southwest Pacific

Tonga-Kermadec is shown in Figure 10, including the Vanuatu and Solomon Islands zones. The base model shows a linear positive anomaly along the trench, yet the same linear trend is not present in MF7. Adding the subduction model weakens this anomaly, suggesting that there is some cancelation between the anomaly from subduction and that associated with juxtaposition of old oceanic lithosphere with crust of the arc and back-arc basin. The observations are unclear: There are large anomalies, but they are not obviously associated with the subduction geometry, and while adding magnetization along the subduction zone can reduce the RMS mismatch with MF7 (Figure 4), the large positive anomaly that spans the Tonga-Kermadec trench and South Fiji Basin is still not well reproduced. Addition of magnetization to the Solomons slab, a narrow structure located close to the magnetic equator, does little to change the modeled anomaly pattern. The Vanuatu slab is also narrow but lies further from the magnetic equator. The base model produces a positive anomaly, which corresponds well to an anomaly in the MF7 map, but again with the wrong sign. Adding magnetization at the location of the slab reverses the sign to agree with MF7.

### 3.7. Northwest Pacific

Figure 11 shows results for subduction zones in the northwest Pacific. The subduction zone from Kamchatka to central Japan has a strong magnetic anomaly. The trench juxtaposes a large region of old seafloor formed during the CNS against back-arc crust; the base model produces a coherent anomaly here but once again with the wrong sign. The sign is reversed by adding magnetization in the region of the slab, while negative anomalies over the Sea of Japan and the Sea of Okhotsk are also reproduced. The Izu-Bonin section has

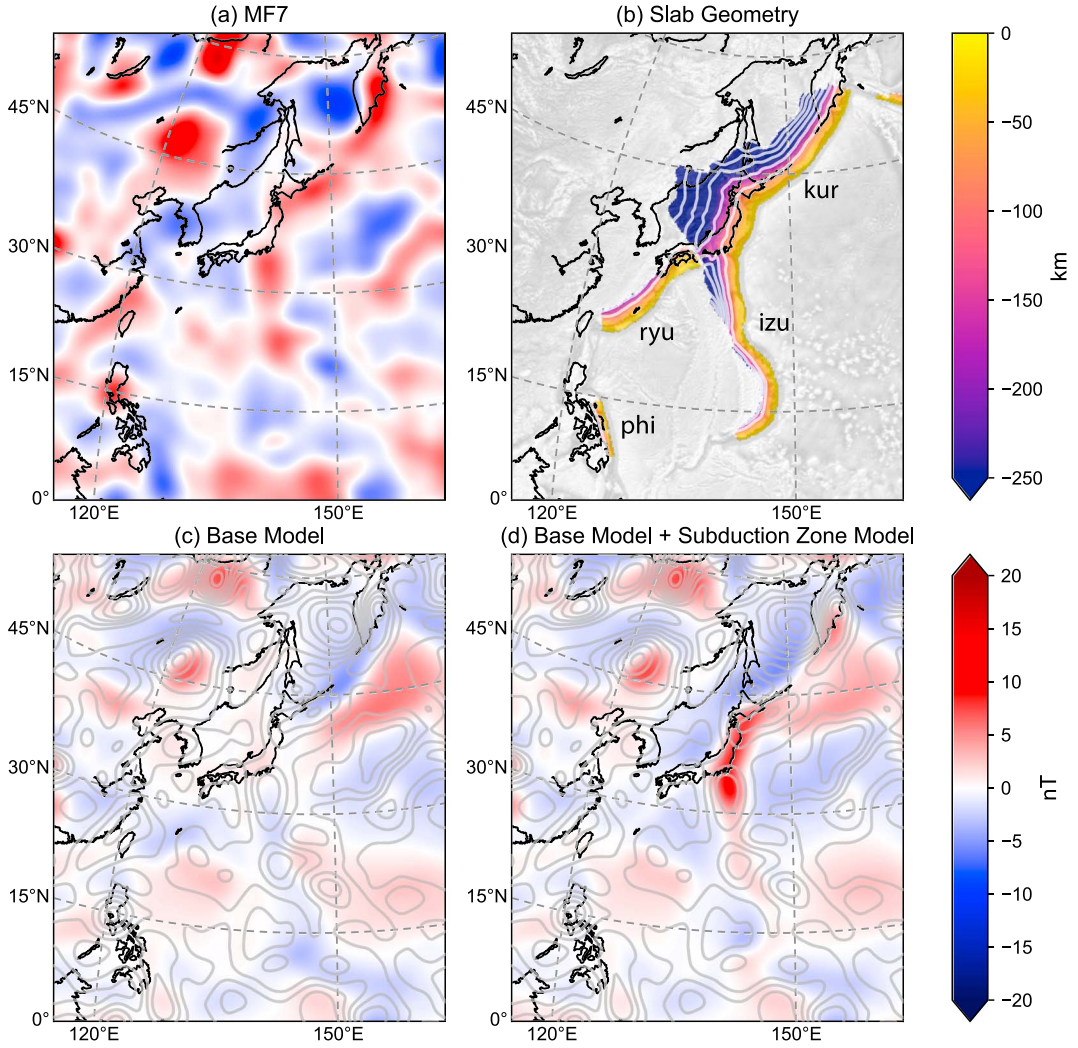


**Figure 11.** As Figure 6 but for the Kamchatka-Kuril-Japan (kur), Izu-Bonin (izu), Ryukyu (ryu), and Philippine (phi) subduction zones.

a relatively weak positive magnetic anomaly in both the data and the subduction zone model, although improvement in the RMS is significant (Figure 4).

The Ryukyu slab is enigmatic—there is no anomaly down the Ryukyu section at all, in agreement with the base model. An anomaly is predicted by subduction models with significant $k$ values such that the RMS reduction (Table 1) is negligible for all values of $k$ and $Z_{\text{lim}}$. The absence of an anomaly at Ryukyu, unlike the case of South America discussed in the next section, is not due to the IVIM being in the null space (supporting information Figure S6); the lack of slab anomaly in Figure 11 is simply the result of a very small optimal susceptibility from Table 1. Finally, there is no direct correspondence between magnetic anomalies in MF7 and the Philippine slab, and RMS values indicate no improvement in the fit by adding any magnetization along this zone, which spans the magnetic equator and lies in the null space.

## 4. Discussion

### 4.1. Evidence for Subduction Zone Magnetization

Systematically adding magnetization to the base model following the locations of presently subducting slabs improves the fit to MF7 magnetic anomalies in most subduction zones. Zones where the improvement is unequivocal have optimum susceptibilities in the range $k = 0.025$ to 0.045 SI (Table 1), assuming a 20-km-thick magnetized layer. Only the product of $k$ and thickness determines the magnetic anomaly, so a

thinner layer would require a higher $k$. This basic result is broadly consistent with previous studies of magnetic anomalies of individual subduction zones, for example, Clark et al. (1985) who have a magnetized 7-km crust with correspondingly higher $k$.

We also wish to determine which part of the subsurface hosts the source of the anomalies. We found the dipping slab model (DVIM) to place the anomaly too close to the trench and can therefore be rejected, although reducing the shallow magnetization and increasing the deeper magnetization might fit the data better. This misplacement can also be observed in the previous studies of the Aleutians (Clark et al., 1985) and Central America (Vasicek et al., 1988), where dipping slab models were used. Counil and Achache (1987) matched the observed anomalies at the Central America subduction zone using a set of horizontal magnetized bodies, all centered landward of the trench. Our results for the UVIM case, which use more recent satellite observations and a magnetization model incorporating other crustal sources, support their finding and suggest that it can be generalized to most present subduction zones.

Although UVIM and IVIM have similar RMS, UVIM requires a greater horizontal extent ($Z_{\text{lim}}$ in Table 1) than IVIM. As with the slab model, UVIM is expected to create an anomaly closer to the trench than IVIM, whose magnetization is concentrated away from the trench. The larger optimum value of $Z_{\text{lim}}$ for UVIM helps move the peak of the anomaly to the right place. Any misplacement would be less than for the slab model because the wedge case has magnetization increasing approximately linearly, while the slab has it decreasing much more rapidly as $(r/r_{\text{E}})^{20}$ (where $r_{\text{E}}$ is the Earth's radius—see section 2).

### 4.2. Discrepancies Between Models and Observations

There are several important discrepancies between models and observations. The most general one is the sign reversal that crops up frequently between the base and subduction models, most clearly apparent in Sumatra, the Aleutians, and Kamchatka-Japan (Figures 6, 7, and 11). Most of the base model anomalies arise from weakly magnetized arc crust (section 2.1.3 and Figure 4 of Hemant & Maus, 2005). These are swamped by the new subduction magnetizations: Our study does not argue against the existence of magnetized arc crust, but the observed anomalies correspond more specifically to present or recent subduction than to arc crust in general.

The magnetic anomalies associated with the Cascadia segment where the Juan de Fuca plate subducts have been extensively studied by Blakely et al. (2005) using higher-resolution aeromagnetic data and we have little to add from our satellite study. Note that their anomaly arises only partly from the serpentinized wedge, the balance being from the continental crust of Cascadia (their Figure 2). The same is true for our model: Only part of the anomaly comes from UVIM, the rest coming from a region where the continental crust in the base model already has a high VIM compared to the surrounding area.

The base model has very little signal along the coast of Central America where the Cocos plate subducts, but the subduction model gives a very satisfactory fit to the Central American Trench. However, it does not contain the strong anomaly running down the Baja California peninsula to the northern tip of the Central America Slab. This suggests that an aseismic subducted slab runs continuously down the coast to join the Central American subduction zone. Some additional evidence exists from seismic tomography for such a slab remnant (Wang et al., 2013). Further north, the observations show no evidence of a subducted slab from Point Conception in California down to Ensenada in Mexico. This is consistent with plate tectonic reconstructions, which conclude that subduction of the Cocos plate ceased there more than 15 Myr ago (Schellart et al., 2010). The change in boundary style from subduction to transform has expanded southward and northward. We propose that the magnetic anomaly from Baja California south is associated with subduction that ceased within the last 15 Myr. Opening of the Gulf of California could destroy the magnetization of the fossil subduction zone by heating, thereby explaining why the Baja anomaly is not fully continuous with the Central American anomaly. The Cascadia magnetic anomaly extends significantly south of the present-day subduction zone, which could also reflect fossil subduction magnetism. Magnetism in the gap where subduction ceased more than 15 Myr ago may have been destroyed by heating due to upwelling or extension.

The slab along the western margin of South America has only a weak anomaly because it trends mostly north-south and is at a relatively low geomagnetic latitude (Arkani-Hamed & Strangway, 1987). In a Cartesian study of induced magnetization using vector cartesian harmonics, Gubbins et al. (2017) showed that

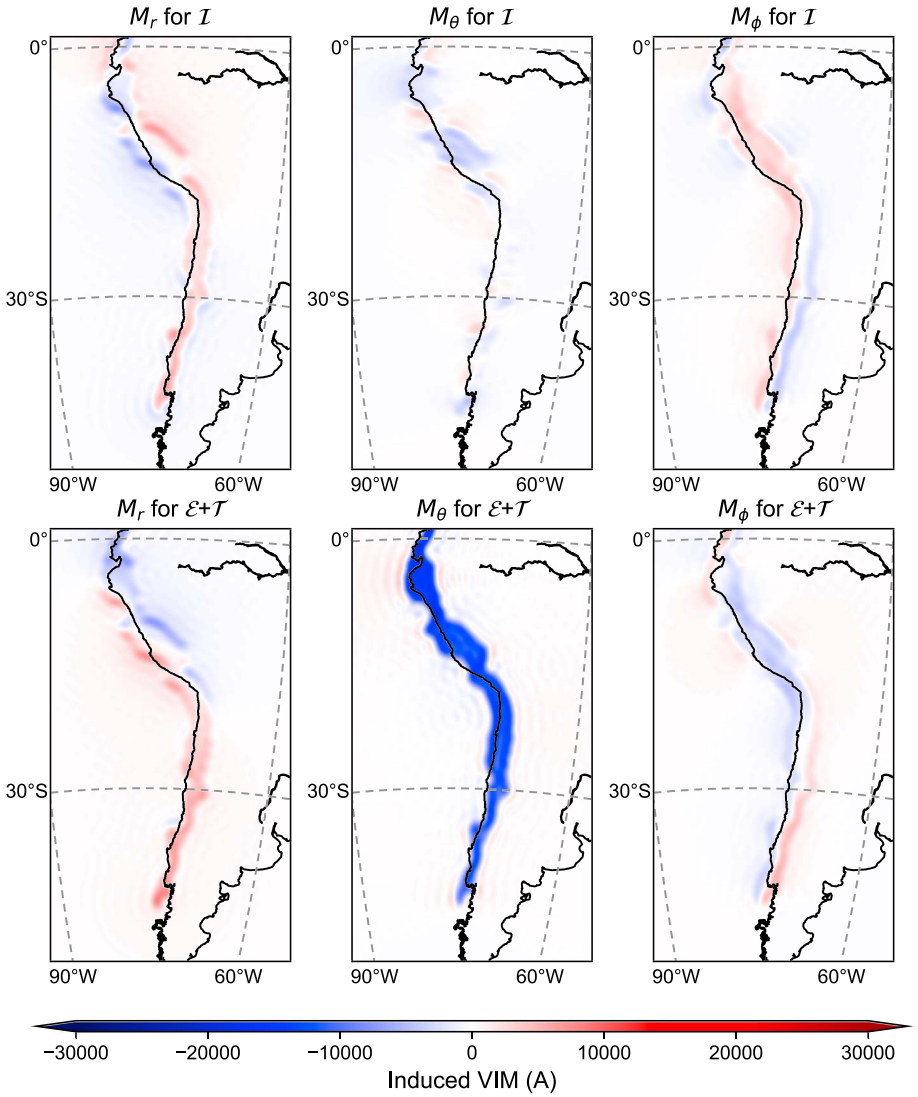


**Figure 12.** Decomposition of the South American subduction magnetization into its vector spherical harmonics components, for UVIM model case with $Z_{\text{lim}} = 100$ km and $k = 0.03$.

2-D magnetizations with strike parallel to a horizontal inducing field gave no observable anomaly. The situation is similar in South America, which we confirm by separating the subduction magnetism into its vector spherical harmonic parts, $\mathcal{I}, \mathcal{E}, \mathcal{T}$ and comparing the visible part $\mathcal{I}$ with the annihilator $\mathcal{E} + \mathcal{T}$. The result is shown in Figure 12 (decompositions for all subduction zones are shown in the supporting information). The upper panels give the visible $\mathcal{I}$ part responsible for the magnetic field. There is some signal in the radial component, but it is weak and weaker than the "invisible" part. The strongest magnetization is in the $M_\theta$, or north-south, component, as expected because the inducing field is mainly horizontal at this low geomagnetic latitude. The north-south component is almost entirely contained in the invisible part and therefore does not contribute to an observable anomaly. The $M_\phi$ component has $\mathcal{I}$ and $\mathcal{E} + \mathcal{T}$ components that are almost equal and opposite to each other so they sum to 0, as required by a north-south inducing field. The split gives a misleading magnetic anomaly in the $\phi$ direction, but it is very weak. The RMS fit in Table 1 shows negligible improvement with respect to the misfit between the base model and MF7 and the optimum susceptibility is very small: Our model anomalies, although weak, do not correlate with the observations well enough to warrant inclusion to the base model. This does not discount other reasons that the magnetic signature of subduction is absent, such as the relative youth of the subducting plate as pointed out by Arkani-Hamed and Strangway (1987).

Tonga-Kermadec has virtually no magnetic anomalies associated with subduction and very little correlation with the slab model. The base model captures some of the features between Australia and New Zealand and to the north, most notably the linear anomaly corresponding to the Vitiaz Trench where old Pacific oceanic lithosphere is juxtaposed against crust of the much younger North Fiji Basin. The addition of slab magnetization improves the fit to MF7 at the Vanuatu arc, but neither the base model nor models incorporating slabs provide an explanation for the positive anomaly observed in the MF7 vertical component across the South Fiji Basin. The $k$ value required for Vanuatu is much higher than for any other zone. This is at least partly due to the base model containing a corresponding anomaly of the wrong sign, which the subduction zone models must compensate for. Additionally, the representation of the Vanuatu zone (in common with the Solomons and Phillipines) in Slab1.0 is much narrower than other zones, so that our VIM models may underestimate the spatial extent (and therefore overestimate $k$).

Kamchatka-Japan and, to a lesser extent, Izu-Bonin are modeled quite well, but there is no anomaly on the Ryukyu trench in the data, whereas one is predicted in the slab model. Although the strike is close to north-south and might be expected, like South America, to be in the null space for a magnetic anomaly, examination of the VSH shows this not to be the case (supporting information Figure S6). Our analysis shows a substantial visible part of the magnetization: Its absence from the model map is because the optimum $k$ (Table 1) is very small, the magnetized zone is simply not needed.

We must seek some other reason that Ryukyu differs from the other zones. Plate reconstructions offer alternative scenarios for the tectonic evolution of this area. Wu et al. (2016) depict the Philippine Sea Plate as subducting at the Ryukyu trench in a fairly consistent fashion for the last 15 Myr following mid-Miocene arc-arc collision, while other reconstructions (Mahony et al., 2011) suggest that much of the plate boundary was characterized by left-lateral transpression prior to 6 Ma. The present slab and wedge may be relatively young and hot in the northeastern part of the trench and therefore relatively unmagnetic, though the same case cannot be clearly made for the southwestern part. Either there is something different about the mineralogy, hydration, or temperature of the seafloor entering this subduction zone that reduces the magnetization or some other feature has a magnetic expression that cancels out the signal expected from the subduction zone.

### 4.3. Origin of Magnetization

So far we have deliberately avoided any direct link to the physical cause of the magnetization and have restricted the models to simple surface functions that stand a chance of being discriminated by the data. We can now discuss implications of the results for these simple structures for likely sources of subduction zone magnetization.

We have been able to rule out the simple DVIM model considered here because it places the anomalies too close to the trench. Both the UVIM and IVIM models fit the data well, and for IVIM the values for $k$ and $Z_{\mathrm{lim}}$ are consistent with the idea of a magnetized mantle wedge. As always with magnetic interpretation, the depth of magnetic anomalies remains unresolved by the data alone.

If magnetization is indeed within the downgoing slab, the magnetization must increase with depth and be absent from shallow areas. Clark et al. (1985) appealed to an increase in $k$ with temperature and pressure in the subducted slab together with an increase in viscous remanent magnetization (VRM). Ocean floor remanent magnetization alternates too rapidly in sign to be seen at satellite altitude but VRM is acquired in the direction of the ambient field and could produce a signal. There is evidence that VRM is acquired faster at higher temperature and may therefore dominate the magnetization in the subducted slabs. Magnetization could be strengthened with pressure (Gilder & Le Goff, 2008) or a phase change, such as that to eclogite. Temperatures and pressures in the shallow part of the slab may be too low to allow enhancement of the magnetization, which could account for absence of magnetism there.

The strength of the magnetic anomalies is determined by the product of $k$ and the assumed thickness of the magnetized region, in our UVIM cases taken as 20 km, and not the individual values. Previous studies have mostly concluded that, in subduction zones, susceptibilities are high but the mineral processes that form magnetite and other magnetic minerals are poorly understood. For example, an extensive study of rocks from the Western Gneiss Region of Norway (McEnroe et al., 2018), which has a large satellite magnetic anomaly, revealed a wide range of metamorphism and magnetic properties that are mostly weaker than is required to explain the observed anomalies. McEnroe et al. (2018) placed bounds on susceptibilities for the

lower crust and upper mantle of 0.01 and 0.04 SI assuming a 15-km-thick layer, which translates to a VIM of 6 to 24 kA. These are comparable with our values but too small for a magnetized dipping slab.

Lower values of susceptibility can be tolerated if the volume of magnetized material is larger. However, previous slab models typically assign the magnetization to lie within a thin layer of oceanic crust. Clark et al. (1985) take 7 km for the thickness of the magnetized layer and require $k \approx 0.1$ to give magnetization 4 A/m to explain the amplitude of the anomalies. Vasicek et al. (1988) vary the thickness of the Central American zone from 4 to 7 km with $k = 0.1$ giving a range of VIM of 20–30 kA. These VIM values are similar to those within our best fitting models for the same subduction zones, but the values of $k$ are high when attributed to a thin layer of oceanic crust and would need to be even higher if the shallow magnetization were placed deeper. The only alternative to very high $k$ is to increase the thickness of the magnetized layer, which would involve extensive magnetization of the upper mantle within the subducted plate.

Invoking magnetization within the mantle wedge allows for a much thicker magnetic layer than the thickness of subducting crust and therefore lower average susceptibility. In the model proposed by Blakely et al. (2005) the mantle wedge can become magnetic by formation of serpentinite, which can contain substantial amounts of magnetite; it is also low density and can therefore rise into the overlying mantle wedge. The relevant thickness is now that of the mantle wedge, and our 20 km can be taken as a guess at the average thickness of the magnetized part of a wedge starting at zero thickness and rising to 40 km, at which point the Curie temperature might be reached. Our optimum susceptibility ($k = 0.02$, Table 1) translates to a magnetization of 0.9 A/m, rather lower than the 1.38 of Blakely et al. (2005) but again their average thickness may be smaller (their Figure 2D). Our values of $k$ are also in line with measurements from serpentinized rock samples (Bonnemains et al., 2016; Klein et al., 2014), with the exception of Vanuatu where the optimum $k$ value is likely to be spuriously high for reasons discussed in section 4.2.

There is good evidence that the temperature of serpentinization exerts a strong control on the magnetic properties of the resulting serpentinite. This has been observed in seafloor hydrothermal vents of different temperatures (Szitkar & Murton, 2018), Ocean Drilling Program samples of serpentinized peridotites (Klein et al., 2014), and ophiolites (Bonnemains et al., 2016). In all cases the critical temperature is 200 °C, below which Fe partitions into brucite rather than magnetite. The shallower regions would not then produce magnetite or a strongly magnetized zone. Based on thermal models of subduction zone temperature (Syracuse et al., 2010), the part of the slab where the top of the slab falls between 200 °C and the Curie temperature will lie within a zone somewhere between 20 and 100 km in depth. By comparison, the best fitting values of $Z_{\mathrm{lim}}$ for our models suggest magnetization is distributed between the trench and where the slab reaches a depth of between 50 and 250 km. This suggests models with $Z_{\mathrm{lim}} \geq 100$ km are unrealistic, which includes UVIM models for the Aleutians and Sumatra and both IVIM and UVIM models for Central America (Table 1). The relevant panels for Figure 4 show that $Z_{\mathrm{lim}}$ could easily be reduced below 100 km for the Aleutians, Central America, and possibly Sumatra without raising the RMS much. Nevertheless, the high values of $Z_{\mathrm{lim}}$ still mitigate in favor of the IVIM model.

We introduced the uniform model UVIM as a simple intermediate case without invoking a single, specific physical justification. Such a uniform layer could perhaps be formed by serpentinite at the top of the wedge region. This raises the interesting question of whether fluids from deeper, hotter parts of the wedge could rise and produce serpentinite in cooler parts of the wedge that contribute to the magnetic anomaly. It would then be possible to have a UVIM $Z_{\mathrm{lim}}$ well above 100 km. The same applies to the IVIM model because fluids may rise from the cool slap top into a hotter wedge region that is above the Curie temperature then further into cooler upper regions. The distinction between IVIM and UVIM is therefore rather blurred.

Regardless of exactly where the magnetization lies within the slab or wedge, the results suggest that zones where subduction has been ongoing for a long period of geological time will retain a magnetic anomaly. When subduction ceases, magnetic anomalies can persist as long as the magnetized material within the fossil slab or cold nose of the wedge remains below the Curie isotherm. In western North America, dehydration of a fossil serpentinized wedge is thought to be ongoing beneath the San Andreas fault in an area where subduction ceased 20 Myr ago (Fulton & Saffer, 2009; Becken & Ritter, 2012). Since the subduction persisted until more recently beneath Baja, this raises the possibility that the long-wavelength anomaly in this region reflects a similar relict serpentinized wedge above the fossil slab identified by Wang et al. (2013). Gaps in the magnetic anomalies further north along the western margin of North America fall within areas where

subduction ceased 30–50 Myr ago, so that magnetized wedges previously existing in these regions have been heated and/or dehydrated sufficiently for their signals to be destroyed.

## 5. Conclusions

Long-wavelength magnetic anomalies at subduction zones can be explained in most cases by magnetization located within the regions of the slab defined by seismicity and tomography. South America has been shown to have no anomaly because the magnetization associated with the subduction zone lies in the null space and produces little external potential field Tonga-Kermadec has a weak anomaly overwhelmed by magnetized bodies associated with anomalous ocean floor throughout the region. The Ryukyu section of the Japan system has no anomaly, perhaps because current subduction began too recently for extensive magnetization due to serpentinization to have formed. Our models indicate that the magnetization lies between the trench and where the slab is 25 to 250 km deep and that the required susceptibility is in the range 0.025–0.045 SI for a magnetized layer thickness of 20 km. Magnetizing the mantle wedge or flat layer located at the "cold nose" of the wedge matches the anomalies better than magnetizing the dipping slab, which places the anomaly too close to the trench. Magnetic anomalies not associated with active seismic zones can reveal the presence of fossil slabs or inactive subduction zones, such as north of the Aleutians and along the Baja California peninsula to Cabo Corrientes in Mexico.

We have relied on satellite data since they provide a uniform coverage across all subduction zones. These data avoid complications associated with constraining long-wavelength signals across continent-ocean boundaries from terrestrial compilations where airborne and marine surveys are stitched together. Rather than pursuing more complex models using satellite data, a better understanding of subduction zone magnetization could be achieved by more detailed regional modeling, similar to that carried out by Blakely et al. (2005) for Cascadia, where additional types of data may be available. Near-surface magnetic data and gravity can account for the expected decrease in density that accompanies serpentinization; decreases in seismic velocity, increasing Poisson ratio, characteristic changes in the reflectivity of the subarc seismic Moho, and increasing electrical conductivity (Hyndman & Peacock, 2003) can also be used to map serpentinization in the mantle wedge. Our global model can be used as a starting point for these regional studies.

**Acknowledgments**
We are grateful to Fabio Speranza and Foteini Vervelidou for thoughtful reviews and thank Sheona Masterton for providing data files and help deriving model output. S. W. was supported by SIEF Project RP 04-174 and ARC Grant IH130200012. The magnetic field model used for this study is available at the http://www.geomag.org/models/MF7.html website. The subduction zone geometries used to construct magnetization models are available at the USGS website (https://earthquake.usgs.gov/data/slab/).

## References

Arkani-Hamed, J., & Strangway, D. W. (1987). An interpretation of magnetic signatures of subduction zones detected by Magsat. *Tectonophysics*, *133*, 45–55. https://doi.org/10.1016/0040-1951(87)90279-4

Becken, M., & Ritter, O. (2012). Magnetotelluric studies at the San Andreas fault zone: Implications for the role of fluids. *Surveys in Geophysics*, *33*(1), 65–105.

Blakely, R. J., Brocher, T. M., & Wells, R. E. (2005). Subduction-zone magnetic anomalies and implications for hydrated forearc mantle. *Geology*, *33*(6), 445.

Bonnemains, D., Carlut, J., Escartín, J., Mével, C., Andreani, M., & Debret B. (2016). Magnetic signatures of serpentinization at ophiolite complexes. *Geochemistry, Geophysics, Geosystems*, *17*, 2969–2986. https://doi.org/10.1002/2016gc006321

Clark, D. (1997). Magnetic petrophysics and magnetic petrology: Aids to geological interpretation of magnetic surveys. *AGSO Journal of Australian Geology and Geophysics*, *17*, 83–104.

Clark, D. A., & Emerson, D. W. (1991). Notes on rock magnetization characteristics in applied geophysical studies. *Exploration Geophysics*, *22*, 547–555.

Clark, S. C., Frey, H., & Thomas, H. H. (1985). Satellite magnetic anomalies over subduction zones: The Aleutian Arc anomaly. *Geophysical Research Letters*, *12*, 41–44. https://doi.org/10.1029/gl012i001p00041

Counil, J.-L., & Achache, J. (1987). Magnetization gaps associated with tearing in the Central America subduction zone. *Geophysical Research Letters*, *14*, 1115–1118.

Counil, J. L., Cohen, Y., & Achache, J. (1991). The global continent-ocean magnetization contrast. *Earth and Planetary Science Letters*, *103*(1-4), 354–364.

Finlay, C. C., Maus, S., Beggan, C. D., Bondar, T. N., Chambodut, A., Chernova, T. A., Chulliat, A., Golovkov, V. P., Hamilton, B., Hamoudi, M., Holme, R., Hulot, G., Kuang, W., Langlais, B., Lesur, V., Lowes, F. J., Lhr, H., Macmillan, S., Mandea, M., McLean, S., Manoj, C., Menvielle, M., Michaelis, I., Olsen, N., Rauberg, J., Rother, M., Sabaka, T. J., Tangborn, A., Tffner-Clausen, L., Th-bault, E., Thomson, A. W. P., Wardinski, I., Wei, Z., & Zvereva, T. I. (2010). International Geomagnetic Reference Field: The eleventh generation. *Geophysical Journal International*, *183*(3), 1216–1230.

Frey, H. (1982). MAGSAT scalar anomaly distribution: The global perspective. *Geophysical Research Letters*, *9*, 277–280.

Fulton, P. M., & Saffer, D. M. (2009). Potential role of mantle-derived fluids in weakening the San Andreas fault. *Journal of Geophysical Research*, *114*, B07408. https://doi.org/10.1029/2008JB006087

Gilder, S. A., & Le Goff, M. (2008). Systematic pressure enhancement of titanomagnetite magnetization. *Geophysical Research Letters*, *35*, L10302. https://doi.org/10.1029/2008gl033325

Gubbins, D., Ivers, D., Masterton, S. M., & Winch, D. E. (2011). Analysis of lithospheric magnetisation in vector spherical harmonics. *Geophysical Journal International*, *187*, 99–117.

Gubbins, D., Ivers, D. J., & Williams, S. (2017). Analysis of regional crustal magnetization in Vector Cartesian Harmonics. *Geophysical Journal International*, *211*(3), 1285–1295.

Hayes, G. P., Wald, D. J., & Johnson, R. L. (2012). Slab1.0: A three-dimensional model of global subduction zone geometries. *Journal of Geophysical Research*, *117*, B01302. https://doi.org/10.1029/2011JB008524

Hemant, K., & Maus, S. (2005). Geological modeling of the new CHAMP magnetic anomaly maps using a geographical information system technique. *Journal of Geophysical Research*, *110*, B12103. https://doi.org/10.1029/2005JB003837

Hunt, C. P., Moskowitz, B. M., & Banerjee, S. K. (1995). Magnetic properties of rocks and minerals. In T.C. Ahrens (Ed.), *AGU Reference Shelf 3, Rock Physics and Phase Relations* (pp. 182–204): American Geophysical Union.

Hyndman, R. D., & Peacock, S. M. (2003). Serpentinization of the forearc mantle. *Earth and Planetary Science Letters*, *212*(3-4), 417–432.

Kincaid, C., & Sacks, I. S. (1997). Thermal and dynamical evolution of the upper mantle in subduction zones. *Journal of Geophysical Research*, *102*, 12,295–12,315.

Klein, F., Bach, W., Humphris, S. E., Kahl, W. A., Jons, N., Moskowitz, B., & Berquo, T. S. (2014). Magnetite in seafloor serpentinite—Some like it hot. *Geology*, *42*(2), 135–138.

Mahony, S., Wallace, L., Miyoshi, M., Villamor, P., Sparks, R., & Hasenaka, T. (2011). Volcano-tectonic interactions during rapid plate-boundary evolution in the Kyushu region, SW Japan. *Geological Society of America Bulletin*, *123*(11-12), 2201–2223.

Masterton, S. M., Gubbins, D., Muller, R. D., & Singh, K. H. (2013). Forward modelling of oceanic lithospheric magnetization. *Geophysical Journal International*, *192*, 951–962.

Maus, S., & Haak, V. (2003). Magnetic field annihilators: Invisible magnetization at the magnetic equator. *Geophysical Journal International*, *155*, 509–513.

Maus, S., Yin, F., Lühr, H., Manoj, C., Rother, M., Rauberg, J., et al. (2008). Resolution of direction of oceanic magnetic lineations by the sixth-generation lithospheric magnetic field model from champ satellite magnetic measurements. *Geochemistry, Geophysics Geosystems*, *9*, Q07021. https://doi.org/10.1029/2008gc001949

McEnroe, S. A., Robinson, P., Church, N., & Purucker, M. (2018). Magnetism at depth: A view from an ancient continental subduction and collision zone. *Geochemistry, Geophysics, Geosystems*, *19*, 1123–1147. https://doi.org/10.1002/2017gc007344

Nataf, H.-C., & Ricard, Y. (1996). 3SMAC: An a priori tomographic model of the upper mantle based on geophysical modeling. *Physics of the Earth and Planetary Interiors*, *95*(1-2), 101–122.

Runcorn, S. (1975). On the interpretation of lunar magnetism. *Physics of the Earth and Planetary Interiors*, *10*, 327–335.

Schellart, W. P., Stegman, D. R., Farrington, R. J., Freeman, J., & Moresi, L. (2010). Cenozoic tectonics of western North America controlled by evolving width of Farallon Slab. *Science*, *329*(5989), 316–319.

Syracuse, E. M., van Keken, P. E., & Abers, G. A. (2010). The global range of subduction zone thermal models. *Physics of the Earth and Planetary Interiors*, *183*, 73–90.

Szitkar, F., & Murton, B. J. (2018). Near-seafloor magnetic signatures unveil serpentinization dynamics at ultramafic-hosted hydrothermal sites. *Geology*, *46*(12), 1055–1058.

ter Maat, G. W., McEnroe, S. A., Church, N. S., & Larsen, R. B. (2019). Magnetic mineralogy and petrophysical properties of ultramafic rocks: Consequences for crustal magnetism. *Geochemistry, Geophysics, Geosystems*, *20*, 1794–1817. https://doi.org/10.1029/2018gc008132

Vasicek, J. M., Frey, H. V., & Thomas, H. H. (1988). Satellite magnetic-anomalies and the Middle America trench. *Tectonophysics*, *154*, 19–24.

Wang, Y., Forsyth, D. W., Rau, C. J., Carriero, N., Schmandt, B., Gaherty, J. B., & Savage, B. (2013). Fossil slabs attached to unsubducted fragments of the Farallon plate. *Proceedings of the National Academy of Sciences*, *110*(14), 5342–5346.

Wu, J., Suppe, J., Lu, R., & Kanda, R. (2016). Philippine Sea and East Asian plate tectonics since 52 Ma constrained by new subducted slab reconstruction methods. *Journal of Geophysical Research: Solid Earth*, *121*, 4670–4741. https://doi.org/10.1002/2016JB012923